Applied Catalysis A: General 388 (2010) 202–210

Contents lists available at ScienceDirect

Applied Catalysis A: General

journal homepage: www.elsevier.com/locate/apcata

Effect of gallia doping on the acid–base and redox properties of ceria

Sebastián Collins[a,*], Gisela Finos[a], Rodrigo Alcántara[b], Eloy del Rio[c], Serafín Bernal[c], Adrian Bonivardi[a]

[a] Instituto de Desarrollo Tecnológico para la Industria Química (INTEC) UNL-CONICET, Güemes 3450, 3000, Santa Fe, Argentina
[b] Dpto. de Física, Facultad de Ciencias, Universidad de Cádiz, Puerto Real, E11510, Spain
[c] Dpto. de Ciencias de los Materiales, Ingeniería Metalúrgica y Química Inorgánica, Facultad de Ciencias, Universidad de Cádiz, Puerto Real, E11510, Spain

ARTICLE INFO

Article history:
Received 8 April 2010
Received in revised form 21 August 2010
Accepted 25 August 2010
Available online 29 September 2010

Keywords:
Cerium oxide
Gallium oxide
Acid–base
Redox
Infrared

ABSTRACT

This work presents the synthesis and characterization of cerium oxide doped with gallium, which were prepared by co-precipitation in basic aqueous solution followed by calcination at 773 K. XRD and Raman spectroscopy suggested that Ga(III) cations were incorporated into the ceria crystal structure. Moreover, surface Ga-H species were detected by FTIR with a 100 cm^{-1} downshift of the ν(Ga-H) peak, which indicated that Ga(III) were incorporated onto the surface lattice of the ceria. Results of CO_2 and CO chemisoption, as well as, TPR-H_2 and TPR-CO, showed that the acid–base (decreased basicity) and redox (enhanced reducibility) properties of the gallium-doped ceria materials were modified as compared with the pure cerium dioxide. The catalytic oxidation of CO was investigated over the oxides.

1. Introduction

Cerium dioxide is known to be widely used as a component or an active phase in numerous redox catalytic processes [1]. Among many other important reactions, ceria-supported noble metal (Au, Pt) materials are promising catalysts for low-temperature water gas shift (LTWGS) reaction, and selective oxidation of CO in the presence of a large excess of H_2 (PROX), two key processes in high purity hydrogen generation reformers for fuel cell applications [2–4]. Two major reasons justify the relevance in catalysis of ceria, the ability to rapidly exchange oxygen with the chemical environment, with parallel and reversible shift of the cerium redox state (Ce^{4+}/Ce^{3+}), and the mobility of O^{2-} exhibited by its fluorite-type structure.

A major problem currently found in the ceria-based catalysts for hydrogen production mentioned above is their progressive deactivation under reaction conditions [5]. Among several others [6], poisoning effects due to carbonate species strongly adsorbed on the ceria surface, have been considered a major cause of deactivation [5,7,8]. Therefore, the development of alternative ceria-based oxide supports forming more labile carbonate species, while keeping the appropriate redox behavior, represents an appealing target for research.

Doping ceria with alio-cations is known to be an efficient and versatile way of modulating the textural, structural and chemical properties of the pure oxide [9]. Though, as indicated in ref [9], ceria–zirconia mixed oxides have received a very special attention, several other cerium-containing mixed oxides have also been investigated. In most of cases, however, the doping cations consisted of lanthanoids and closely related elements like yttrium [9]. More recently, Auroux et al. [10,11] have reported the preparation and characterization of a series of ceria-based mixed oxides including in their formulation B_2O_3, Al_2O_3, Ga_2O_3 and In_2O_3. As deduced from [10,11], the incorporation of these elements into the ceria lattice may induce some interesting modifications in the chemical properties of pure ceria. This prompted us to initiate a research project aimed at evaluating the textural, structural, acid–base, and redox properties of materials resulting from the gallia doping of cerium dioxide.

Three major reasons justify our choice of the ceria–gallia system. First, some of us have been working on the chemical characterization of gallium oxides polymorphs [12]. As revealed by the FTIR studies reported in [12], up to six carbonate species showing a poor thermal stability have been observed to occur on these gallia polymorphs. In fact, most of them are easily removed by simple outgassing at room temperature [12]. Second, gallium oxide is able to dissociatively chemisorbs hydrogen at temperatures higher than 523 K producing $Ga^{\delta+}$-H surface species [13,14]. It was also found that $Ga^{\delta+}$-H species are able to stepwise reduce CO_2 adsorbed as carbonate to formate, methylenebisoxy and methoxy [15]. Third, the general information about Ce–Ga mixed oxides should be

* Corresponding author.
E-mail address: scollins@santafe-conicet.gov.ar (S. Collins).

0926-860X/$ – see front matter © 2010 Elsevier B.V. All rights reserved.
doi:10.1016/j.apcata.2010.08.050

considered rather scarce [10,11]. In the specific case of redox properties, no detailed data are to our knowledge available.

2. Experimental

2.1. Sample preparation

In this work, four different oxide samples have been prepared and characterized. Two of them were Ce–Ga mixed oxides, with the nominal composition $Ce_{0.75}Ga_{0.25}O_{1.875}$. The remaining two samples consisted of pure cerium and gallium oxides used as reference systems.

The ceria–gallia mixed oxides were prepared by precipitation with ammonium hydroxide (14 wt%) from the appropriate solution in purified water (18 ΩM) of the corresponding nitrates, $Ce(NO_3)_3{\cdot}6H_2O$ (99.99%, Aldrich) and $Ga(NO_3)_3{\cdot}9H_2O$ (99.999%, Aldrich). Two alternative precipitation procedures have been followed: (i) direct co-precipitation (labeled CeGa-DC), in which ammonia solution was dropwise added to the Ce^{3+} and Ga^{3+} nitrate solution under vigorous stirring, until the precipitation was completed (pH 8); and (ii) inverse co-precipitation (labeled CeGa-IC), where the cationic solution was dropwise added to the ammonia solution (pH 10), keeping the pH controlled in the range of 8.0–8.5 by co-adding aqueous ammonia solution (14 wt%). Precipitation was always carried out at room temperature. The resulting solids were immediately filtered, washed with purified water, dried in air at 343 K for 8 h, and finally calcined at 773 K for 5 h.

Pure CeO_2 was obtained by following the direct precipitation procedure applied to the preparation of the so-called CeGa-DC mixed oxide. Filtering, drying and calcination routines were the same as those applied to the preparation of the Ce–Ga mixed oxides. Pure γ-Ga_2O_3 phase was synthesized following the procedure reported elsewhere [13]. Hydrated gallium hydroxide gel was obtained from the addition of an ammonia ethanolic solution (14 wt%) to a solution of $Ga(NO_3)_3{\cdot}9H_2O$ in ethanol. This gel was filtered and washed with ethanol at room temperature. The preparation procedure was completed by applying the same drying at 343 K (8 h), and calcination at 773 K (5 h) routines mentioned above.

2.2. Characterization

The structural nature of the phases present in the calcined samples was determined by X-ray diffraction spectrometry (XRD). A Shimadzu XD-D1 apparatus (Cu Kα radiation, 0.125°/min) was used in these studies.

A Micromeritics Accusorb 2000E instrument was used to measure the Brunauer–Emmett–Teller (BET) surface area (S_{BET}) of the oxides. Prior to running the N_2 adsorption isotherms at 77 K, samples were outgassed at 473 K for 3 h under dynamic vacuum (base pressure = 1×10^{-4} Torr).

The Raman spectra were collected using an ad-hoc configuration, equipped with an excitation laser DPSS from Oxxius with an emission line at 532 nm, a dispersion system with double monochromator (Jobin-Yvon model U1000), in an additive asymmetric configuration Czerny-Turner and a photomultiplier detector (Hamamatsu R-943). Spectra were collected at a resolution of 1.5 cm^{-1} with an acquisition time of 60 min.

CO_2 and CO adsorption, at 298 K, was investigated by in situ transmission Fourier transform infrared (FTIR) spectroscopy on self-supported wafers (30 mg) of the oxide samples pressed at 5 ton cm^{-2} (wafer diameter = 13 mm). The sample disks were placed into a Pyrex IR cell fitted with water-cooled NaCl windows, which was attached to a conventional high vacuum system (base pressure = 1×10^{-4} Torr), equipped with a manifold for gas flow operation. Before the adsorption of CO or CO_2, the sample were cleaned as follows: (1) heating from 298 to 723 K (10 K min^{-1}) in a flow of pure H_2 (50 cm^3 min^{-1}), (2) evacuation at 723 K during 15 min; (3) re-oxidation under flowing O_2 (50 cm^3 min^{-1}) at 723 K for 15 min, (4) cooling to 398 K still under oxygen flow, (5) evacuation at 398 K during 25 min, and (6) cooling to 298 K under dynamic vacuum. This cleaning procedure was considered to be the best option to thoroughly remove the surface carbonates from these oxide materials. Adsorption isotherms were recorded at 298 K by progressively increasing the CO_2 (CO) partial pressure up to 760 Torr.

CO_2 and CO adsorption at 298 K was also investigated by using a micro-reactor coupled on-line with a Balzers QMG 421 quadrupole mass spectrometer. Approximately 200 mg of the oxide samples diluted with 200 mg of crushed quartz, 80-30 mesh, were first submitted to a cleaning procedure similar to that reported above, in which steps 2, 5 and 6 consisted of treatments under flowing He, instead of high vacuum. The amount of adsorbed CO_2 or CO on the oxides was determined at 298 K after switching a chromatographic valve from pure He to 5% CO_2/Ar or 5% CO/Ar (10 cm^3 min^{-1}). The total CO_2 or CO uptake (Q), under a partial pressure of 37 Torr of the adsorbate (equilibrium condition), was determined by taking the integral of the difference between the trace of the adsorbate during the adsorption experiment (curve_ads) and the trace of a blank experiment (curve_blank), for a given gas molar flow rate of the adsorbate (F) and weight of sample (W) from $t = 0$ s to $t = 300$ s.

$$Q = \int_0^t (\text{curve\_ads} - \text{curve\_blank}) \frac{F}{W}\, dt$$

After the previous CO_2 adsorption experiments, each sample was purged with flowing He (50 cm^3 min^{-1}) for 20 min, at 298 K, and then a temperature-programmed desorption experiment (TPD-CO_2) was carried out at 10 K min^{-1} from 298 up to 723 K.

H_2 (or D_2) adsorption isotherms were also recorded by using FTIR spectroscopy. The cleaning procedure included the steps 1 through 3 described above; then the samples were evacuated at 723 K for 20 min, and finally pure H_2 (or D_2) was flowed through the infrared cell (50 cm^3 min^{-1}), at 723 K for 15 min. FTIR spectra were also collected at 723 K. When needed, background correction was achieved by subtracting the spectra recorded for the pretreated wafers prior to any contact with H_2 (D_2).

The redox properties of the oxide samples were studied by temperature-programmed reduction-mass spectrometry (TPR-MS). The experiments were performed on 200 mg of sample placed in an U-shaped quartz reactor. The evolved gases were analyzed with a Pfeiffer Thermostar quadrupole mass spectrometer. Prior to running the TPR experiments, the oxides were submitted to a cleaning procedure similar to that reported in [16]. It consisted of heating the oxides in a flow of 5% O_2/He (50 cm^3 min^{-1}) at 773 K (1 h), followed by cooling to 473 K under the oxidizing mixture, and further to 298 K in a flow of He (20 cm^3 min^{-1}). Both diluted hydrogen, 5% H_2/Ar, and carbon monoxide, 5% CO/He, were used as reducing agents (hereafter, TPR-H_2 and TPR-CO, respectively). The flow rate was 50 cm^3 min^{-1}, and the heating rate from 298 to 1273 K was 10 K min^{-1}.

The catalytic activity for CO oxidation was measured using 55 mg of each sample in a fixed bed glass tubular microreactor (i.d. = 7 mm). The composition of the reaction mixture was 1% CO + 20% O_2 balanced with He (total flow = 60 cm^3 min^{-1}). Light-off curves were performed from 300 to 873 K (10 K min^{-1}). The gases at the outlet of the reactor were analyzed with a Pfeiffer Prisma mass spectrometer. Prior to the study of the catalytic activity, each sample was pretreated at 523 K in an oxidizing atmosphere under flow of 5% O_2/He (60 cm^3 min^{-1}) for 1 h and then under flow of He (60 cm^3 min^{-1}) also during 1 h.

Table 1
Chemical analysis, crystal structure and BET surface area of investigated samples.

Sample	Molar nominal Ce/Ga ratio	Ga[a] (wt %)	Crystal phase (XRD)	Mean crystal size[b] (nm)	Lattice parameter, a (nm)	BET surface area ($m^2\,g^{-1}$)
CeO_2	100/0	0	Cubic fluorite (*Fm3m*)	9.34	0.541	83
CeGa-DC	75/25	11.3 ± 1.9	Cubic fluorite (*Fm3m*)	4.07	0.537	95
CeGa-IC	75/25	11.5 ±1.6	Cubic fluorite (*Fm3m*)	4.01	0.536	107
γ-Ga_2O_3	0/100	–	Gamma (*Fd3m*)	1.86	–	126

[a] As determined by flamme atomic emission spectrophotometry.
[b] As determined from line broadening of XRD peaks.

All the gases used in this work were high purity grade and were further purified as follows: H_2 (AGA, 99.999%), He (AGA, 99.998%), and CO_2 (AGA, 99.996%) were passed through MnO/Al_2O_3 and molecular sieve (3 Å, Fisher Co.) traps to eliminate oxygen and water impurities, respectively; O_2 (AGA, 99.999%) was passed through a molecular sieve (3 Å, Fisher Co.) and Ascarite traps to remove water and carbon dioxide, respectively. Additionally, a liquid nitrogen tramp was used for H_2 (D_2) chemisorption experiments.

3. Results and discussion

3.1. Structural characterization studies

Table 1 summarizes the chemical composition and textural properties of the four investigated samples. In the case of the mixed oxides, the Ce/Ga molar ratio in the nitrate solution of the precursor and those determined for the calcined oxide samples are in good agreement, thus indicating that neither DC nor IC preparation routines induce any significant deviation of the oxide composition with respect to the nominal values. Table 1 also shows that all the samples have relatively high surface areas, and that Ga(III) addition to cerium oxide seems to increase approximately 20% the surface area of the pure ceria. However, based on the molecular weight of the oxides (152.5 and 172.1 g mol^{-1} for $Ce_{0.75}Ga_{0.25}O_{1.875}$ and CeO_2, respectively), the values of BET surface areas can now be corrected to express the surface area per mol of oxide. The average ratio between these areas is 1.08 (very close to the unit, based on experimental errors), which suggest that the new molecular surface areas of CeO_2 and $Ce_{0.75}Ga_{0.25}O_{1.875}$ are quite similar.

Fig. 1 summarizes the powder XRD patterns for the investigated samples. Pure ceria shows the characteristic peaks of a cubic, fluorite-type, structure (JCPDS 34-0394). Regarding pure gallia, the diagram consists of broad diffraction peaks which may all be assigned to the γ-polymorph with cubic spinel-type structure, space group *Fd3m* [13,17]. In the case of the Ce–Ga mixed oxide samples, the only diffractions peaks that could be identified are those due to the fluorite structure. Likewise, as deduced from their full width at half maxima, peaks in ceria–gallia patterns are significantly broader than those for pure ceria, indicating smaller mean crystal size in the mixed oxide samples (Table 1).

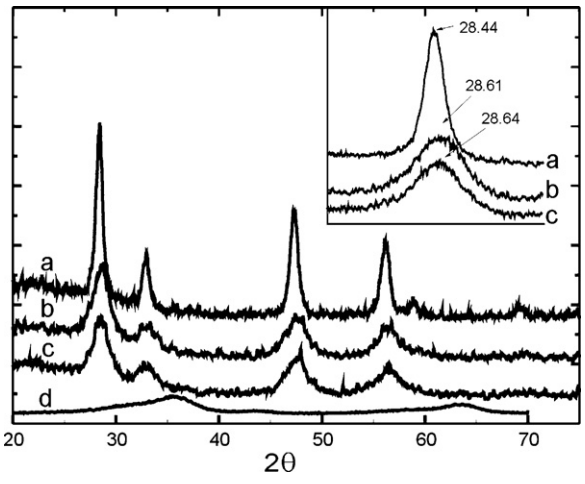

Fig. 1. X-ray diffraction pattern for CeO_2 (a), CeGa-DC (b), CeGa-IC (c) and γ-Ga_2O_3 (d) samples.

The comparison between the peak position in the XRD diagrams for the mixed oxides and pure ceria does also deserves some comment. As clearly seen in the inset of Fig. 1, in which (1 1 1) diffraction peaks for CeO_2, CeGa-DC and CeGa-IC are reported, a shift to higher 2θ values can be observed in the latter. It is well known that the incorporation of alio-cations into the host lattice of an oxide may modify its lattice parameters according to the Vegard's rule [1]. In the case of doped-ceria systems, the following empiric relationship has been established [18]:

$$a = 0.541134 + (0.00220\Delta r_k + 0.00015\Delta z_k)m_k \quad (1)$$

where a (nm) stands for the lattice constant of the ceria solid solution; Δr_k (nm) stands for the ionic radius difference ($r_k - r_{Ce}$) between the k dopant and Ce^{4+} radius (0.097 nm); Δz_k stands for the valence difference ($z_k - 4$) between the k dopant and the Ce^{4+} ion; and m_k stands for the molar fraction of the k dopant cation. For a Ga^{3+} as a dopant (r_k = 0.062 nm, z_k = 3), equation (1) becomes:

$$a = 0.541134 - 0.000227m_{Ga} \quad (2)$$

Taking into account the observed shift in the (1 1 1) diffraction peaks, which is also expressed in the lattice parameters shown in Table 1, we conclude that the Ga^{3+} cations have been incorporated into the ceria structure leading to mixed oxides with a composition close to the nominal one, that is, $Ce_{0.75}Ga_{0.25}O_{1.875}$. Likewise, no XRD peaks due to pure gallia phases could be observed, which suggests that the co-precipitated Ce–Ga samples mainly consist of mixed oxide phases.

Raman spectroscopy has also provided with valuable structural information about the four investigated oxides. The corresponding spectra are reported in Fig. 2. Regarding the experimental spectrum for our pure gallia sample, it consists of a series of low intensity bands at 528, 615, 760, and 1047 cm^{-1}. This spectrum does not match to any of those reported in the literature [19–22] for α-Ga_2O_3, whose main features are observed at 216, 284, 430, 573, and 689 cm^{-1}, respectively, or for the monoclinic phase, β-Ga_2O_3, at 200, 318, 349, 417, 474, 629, 653, and 766 cm^{-1}. Since the XRD for our gallia sample could be assigned to the γ-phase, we conclude that the recorded Raman spectrum does correspond to this polymorph. To the best of our knowledge, no information on the Raman spectrum for γ-Ga_2O_3 is presently available in the literature.

Raman spectra for the ceria-containing samples consist of a main band at 460.9 cm^{-1} (FWHM = 18.0 cm^{-1}), 460.5 cm^{-1} (FWHM = 19.5 cm^{-1}), and 459.1 cm^{-1} (FWHM = 42.0 cm^{-1}), for CeO_2, CeGa-DC, and CeGa-IC, respectively. This feature may be assigned to the F2g symmetry mode characterizing the cubic fluorite structure. This fundamental vibration, which can be viewed as a symmetric breathing mode of the O^{2-} ions around each Ce^{4+} cation [23] is the only allowed mode for ceria. In good agreement with XRD results commented on above, the Raman spectra for CeGa-DC and

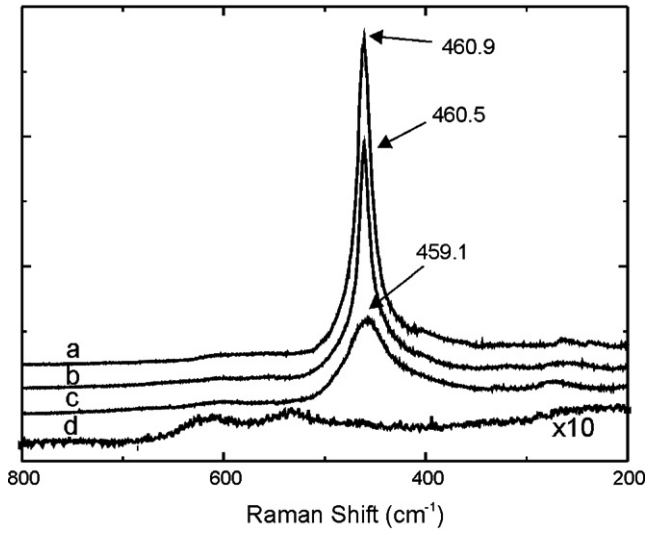

Fig. 2. Raman spectra for CeO_2 (a), CeGa-DC (b), CeGa-IC (c) and γ-Ga_2O_3 (d) samples.

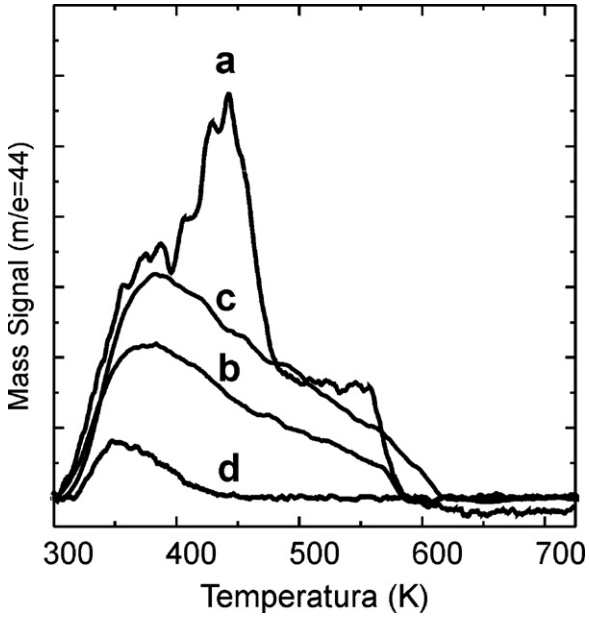

Fig. 3. TPD study of CO_2 pre-adsorbed on CeO_2 (a), CeGa-DC (b), CeGa-IC (c) and γ-Ga_2O_3 (d) samples.

CeGa-IC samples do not show any evidence of bands due to any segregated polymorph of Ga_2O_3, thus confirming that gallium is fully incorporated into the ceria lattice. In addition to the shift towards lower frequency, the band characterizing the Raman spectra for CeGa samples is asymmetric, with a low frequency tail. This tail is interpreted as due to the presence of oxygen vacancies resulting from the doping of ceria with trivalent gallium cations [1,24]. In effect, in accordance with the Kröger–Vink's notation, the incorporation of Ga^{3+} into the CeO_2 lattice can be formulated as follows:

$$0.5xGa_2O_3 + (1-x)CeO_2 \rightarrow xGa'_{Ce} + 0.5xV_{\ddot{O}} + (1-x)Ce_{Ce} + (2-0.5x)O_O \quad (3)$$

where Ga_{Ce}' represents Ga^{3+} in the Ce^{4+} lattice positions, $V_{\ddot{O}}$ represents an oxygen vacancy, and Ce_{Ce} and O_O represent oxygen and cerium at their respective lattice sites.

4. Chemical characterization studies

In addition to the structural studies presented and discussed in the previous section, we have also investigated the effects of gallia doping on the chemical properties of the cerium dioxide. We have paid a special attention to the comparative analysis of the surface chemistry of the investigated oxides. TPD-MS, and FTIR spectroscopy of different probe molecules, H_2, CO and CO_2, have been the experimental tools applied in these studies. Likewise, we have investigated the doping effects on the redox response of ceria against H_2 and CO, two of the most commonly used reducing agents [25,26].

4.1. Adsorption and desorption of carbon oxides

Table 2 reports on the amounts of CO_2 and CO adsorbed on the cleaned oxide samples. The experiments were carried out at 298 K, under dynamic conditions, at a constant partial pressure of adsorbate (either CO_2 or CO) of 37 Torr. As deduced from Table 2, the largest amounts of adsorbed CO_2 (2.87 μmol m^{-2}) and CO (0.44 μmol m^{-2}) are determined for the cerium dioxide. The opposite is true for Ga_2O_3, the sample showing the lowest surface density of adsorption sites for both CO_2 (0.42 μmol m^{-2}) and CO (0.12 μmol m^{-2}). In the case of Ce–Ga mixed oxides, the CO_2 uptakes, 2.17 and 1.96 μmol m^{-2} for CeGa-IC and CeGa-DC, respectively, are approximately a 30% smaller than that determined for pure ceria. The effect of gallia doping is even stronger on the amount of adsorbed CO, 0.17 and 0.27 μmol m^{-2} for CeGa-IC and CeGa-DC, respectively, to be compared with 0.44 μmol m^{-2} for pure ceria. To summarize, the quantitative adsorption studies commented on above show that the incorporation of Ga^{3+} into the ceria lattice leads to materials with intermediate adsorption capabilities with respect to those observed in the pure ceria and gallia. As is known [27,28], CO_2 is a molecule widely used to probe surface basicity of oxides. Therefore, the reported CO_2 adsorption data clearly show that pure ceria is the oxide with the highest surface basicity, it progressively decreasing in the mixed oxides up to reaching a minimum on pure gallia.

After completing the CO_2 chemisorption, the reactor was purged for 20 min with pure He and the corresponding TPD diagrams were recorded. Fig. 3 depicts the desorption traces for pre-adsorbed CO_2. The TPD-CO_2 trace for Ga_2O_3 consists of a very weak peak centered at 350 K, which vanishes at approximately 400 K. The diagram for pure ceria is much broader and intense. It shows at least three distinguishable peaks at approximately 370, 440, and 525 K, that at 440 K showing the highest intensity. As expected from the quantitative CO_2 adsorption data reported in Table 2, the TPD-CO_2 diagrams for CeGa-DC and CeGa-IC account for an intermediate behavior of the mixed oxides against CO_2 adsorption. In accordance with Fig. 3, the traces for CeGa-DC and CeGa-IC are very similar. They consist of a very broad asymmetric peak centered at approximately 370 K, with a long tail on the high-temperature side. They are fully consistent with the occurrence of a significant loss of surface basic sites as gallium ions are incorporated into the ceria lattice. The thermal stability of adsorbed CO_2 on the mixed oxides is also lower than that on pure ceria.

Table 2
Density of CO_2 and CO adsorbed and maximum desorption temperature (T_m) for the desorption products from activated oxides.

Sample	CO_2 (μmol m^{-2})	CO (μmol m^{-2})	T_m CO_2 (K)
CeO_2	2.87	0.44	370, 440, 525
Ga_2O_3	0.42	0.12	350
CeGa-IC	2.17	0.17	370, 525
CeGa-DC	1.96	0.27	370, 525

The adsorption of both carbon dioxide and carbon monoxide was also investigated by in situ FTIR spectroscopy. The isotherm-type experiments were carried out at 298 K. They consisted of a series of spectra recorded at increasing partial pressure of the adsorbate, from 1 to 760 Torr. Fig. 4A shows the spectra taken at the highest CO_2 partial pressure, $P(CO_2) = 760$ Torr, on the four investigated samples. Likewise, Fig. 4B summarizes the adsorption isotherms built up by plotting the total integrated absorbance (normalized by weight and surface area) data for the spectral region ranging from 1800 to 1100 cm^{-1} against the corresponding CO_2 partial pressure at which the spectra were recorded. As deduced from Fig. 4B, Langmuir-type isotherms were obtained on the four oxide samples.

Upon the exposure of the cleaned γ-Ga_2O_3 to 760 Torr of CO_2 at 298 K, several signals evolved in the 1800–1000 cm^{-1}. These observed bands have been previously assigned to bicarbonate species [HCO_3^-: $\nu_{as}(CO_3) = 1630\ cm^{-1}$, $\nu_s(CO_3) = 1420$ and $\delta(OH) = 1225\ cm^{-1}$] and to bidentate carbonate surface groups [b-$CO_3^=$: 1578 and 1310 cm^{-1}] [12]. In good agreement with earlier studies, 20 min evacuation at 298 K produces a strong decrease of the band intensities (Fig. 4C), thus confirming the moderate basicity of surface sites in the gallium oxide [12].

Upon CO_2 adsorption at 298 K, CeO_2 is able to form large amounts of carbonate species. According to Li et al. [29] and Binet et al. [30], these bands can be assigned to different adsorption forms including: (i) bicarbonate [HCO_3^-: $\nu_{as}(CO_3) = 1610\ cm^{-1}$, $\nu_s(CO_3) = 1410\ cm^{-1}$ and $\delta(OH) = 1217\ cm^{-1}$]; (ii) bidentate carbonate [b-$CO_3^=$: $\nu_{as}(CO_3) = 1559\ cm^{-1}$ and $\nu_s(CO_3) = 1290\ cm^{-1}$]; (iii) monodentate carbonate [m-$CO_3^=$: $\nu_{as}(CO_3) = 1465\ cm^{-1}$ and $\nu_s(CO_3) = 1365\ cm^{-1}$]; and polydentate carbonate [p-$CO_3^=$: $\nu_{as}(CO_3) = 1563\ cm^{-1}$ and $\nu_s(CO_3) = 1393\ cm^{-1}$]. About the 60% of the total integrated absorbance of all these bands remained in the spectra after evacuation at room temperature (Fig. 4C), indicating, as expected, the stronger basicity of CeO_2 surface sites, as compared to those found in pure gallia.

Similar spectral features were registered after CO_2 adsorption on the CeGa-DC and CeGa-IC samples. In accordance with Fig. 4A, the carbonate species formed on the mixed oxides show closer analogy with those identified on CeO_2 than on those recorded on Ga_2O_3. Likewise, the FTIR isotherms reported in Fig. 4B show that the amounts of adsorbed CO_2 on the mixed oxides are between those determined for pure ceria and gallia.

The spectra of the evacuated samples at 298 K after the adsorption of CO_2 at 760 Torr, also suggest the presence of surface gallium cations embedded in a ceria matrix. The evacuation of the CeGa-IC sample previously exposed to CO_2 led to a strong decrease of the intensity of the infrared bands due to mainly b-CO_3^{2-} and m-CO_3^{2-} species, but no bicarbonate groups (Fig. 4C). Conversely, after the evacuation of the CeGa-DC sample, most of the bicarbonate species were eliminated from the surface, but bidentated carbonate remained (Fig. 4C). We may conclude accordingly that the preparation method plays a role in determining the surface acid–base properties of the mixed oxides.

The FTIR study of the CO adsorption, at 298 K, on the four investigated oxides is summarized in Fig. 5. Fig. 5B shows the isotherms generated by plotting the total integrated absorbance (normalized by weight and surface area) data for the 1800–1100 cm^{-1} region of the corresponding spectra versus the CO partial pressure.

The FTIR spectrum for CO adsorbed on gallia, Fig. 5A, consists of three main bands which have been previously assigned to bicarbonate species [HCO_3^-: $\nu_{as}(CO_3) = 1630\ cm^{-1}$, $\nu_s(CO_3) = 1420$ and $\delta(OH) = 1225\ cm^{-1}$] [12]. Additionally, two weak bands at 1578 and 1310 cm^{-1} corresponding to bidentate carbonate surface groups (b-$CO_3^=$) [12] may also be observed. All these bands completely disappear after 10 min evacuation at 298 K (Fig. 5C).

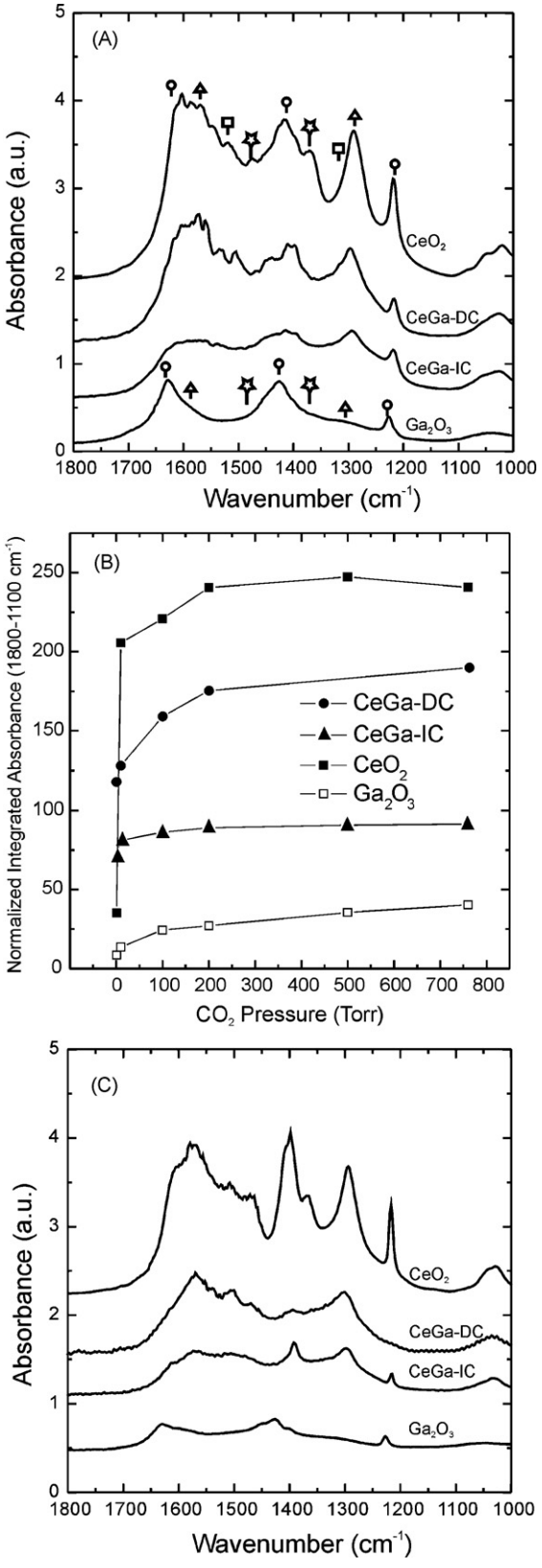

Fig. 4. Infrared spectra for CO_2 adsorption at 760 Torr (A), integrated intensity of carbonate region (1800–1100 cm^{-1}) as a function of the CO_2 pressure (B) and infrared spectra after evacuation at room temperature ($P = 1 \times 10^{-4}$ Torr) (C). Symbols: (○) HCO_3^-, (☆) m-$CO_3^=$/p-$CO_3^=$; (△) b-$CO_3^=$; (□) CO_2^-.

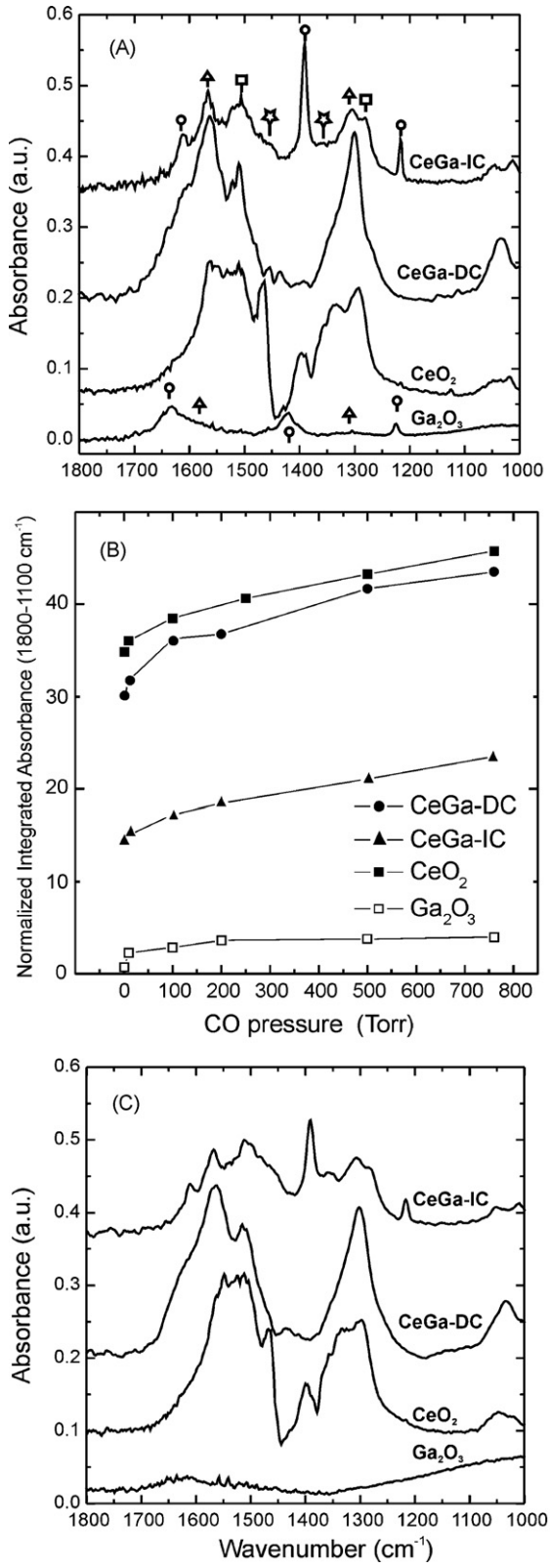

Fig. 5. Infrared spectra for CO adsorption at 760 Torr (A), integrated intensity of carbonate region (1800–1100 cm^{-1}) as a function of the CO pressure (B) and infrared spectra after evacuation at room temperature ($P = 1 \times 10^{-4}$ Torr) (C). Symbols: (○) HCO_3^-, (☆) m-$CO_3^=$/p-$CO_3^=$; (△) b-$CO_3^=$; (□) CO_2^-.

In the case of pure ceria, CO adsorption leads to the onset of a complex series of bands in the 1800–1000 cm^{-1} region of the spectrum (Fig. 5A). With reference to the parallel CO_2 adsorption studies of carbonate species, the amounts resulting from CO adsorption are significantly lower. Again, these bands can be assigned to: (i) bidentate carbonate [b-$CO_3^=$: $\nu_{as}(CO_3) = 1559\ cm^{-1}$ and $\nu_s(CO_3) = 1295\ cm^{-1}$]; (ii) monodentate carbonate [m-$CO_3^=$: $\nu_{as}(CO_3) = 1463\ cm^{-1}$ and $\nu_s(CO_3) = 1334\ cm^{-1}$]; (iii) carboxylate [$CO_2^-$: $\nu_{as}(CO_2) = 1513\ cm^{-1}$ and $\nu_s(CO_3) = 1310\ cm^{-1}$ (very overlaped)]; (iv) bulk or polydentate carbonate [p-$CO_3^=$: $\nu_{as}(CO_3) = 1563\ cm^{-1}$ and $\nu_s(CO_3) = 1393\ cm^{-1}$]; and (v) bicarbonate [$HCO_3^-$: $\nu_{as}(CO_3) = 1634\ cm^{-1}$, $\nu_s(CO_3)$ = not resolved and $\delta(OH) = 1215\ cm^{-1}$] [29,30]. As can be noted in the difference spectra of Fig. 5A, the strong bands due to p-$CO_3^=$ slightly shifted to lower frequency producing the negative feature at 1440 cm^{-1}, since some polydentate carbonate species could not be completely removed by the application of the cleaning routine. After completing the CO isotherm at 760 Torr, the sample was evacuated at 298 K for 20 min. The only bands significantly modified by this treatment were those assigned to m-$CO_3^=$ species (Fig. 5C).

The spectra recorded for CO adsorbed on the cerium-gallium mixed oxide samples show some significant differences from each other, thus reflecting one more time the influence of the preparation procedure on their surface properties. Thus, over CeGa-DC, two intense bands at 1564 cm^{-1} and 1298 cm^{-1} may be noticed. As in the case of pure ceria, these features, which can be assigned to b-$CO_3^=$ species, remain unmodified upon evacuation at 298 K (Fig. 5C). Also, the spectrum recorded for CO adsorbed on CeGa-DC shows the occurrence of stretching bands due to carboxylate groups.

The FTIR spectrum for CO adsorbed on CeGa-IC, Fig. 5A, shows the occurrence of couples of bands at 1566/1303, 1511/1280 and 1460/1355 cm^{-1}, which have a very close resemblance with those assigned to b-$CO_3^=$, CO_2^- and m-$CO_3^=$ species, respectively, on pure CeO_2 [29]. As already noted, the only bands vanishing upon evacuation at 298 K are those attributed to m-$CO_3^=$ surface species (Fig. 5C). This suggests the occurrence of a stronger interaction of the bidentate carbonate species formed on the mixed oxides as compare to that observed on pure gallium or cerium oxides. In addition to the bands mentioned above, the spectrum of CO adsorbed on CeGa-IC shows intense and sharp bands at 1611, 1390, and 1216 cm^{-1}, similar to those observed in the CO-Ga_2O_3 spectrum. They are assigned to HCO_3^- species, but they are clearly shifted toward lower wavenumbers in this mixed oxide. Moreover, on CeGa-IC, these bands are not modified by 20 min evacuation treatment at 298 K (Fig. 5C), which clearly indicates a higher thermal stability of the bicarbonate species adsorbed on the mixed oxide as compared to that observed in pure gallia.

In good qualitative agreement with the results reported in Table 2, the adsorption isotherms shown in Fig. 5B also suggest that the CO adsorption capability of the Ce–Ga mixed oxides is intermediate between the extreme behaviors exhibited by the pure oxides. Additionally, isotherms in Fig. 5B suggest that the amount of CO adsorbed on CeGa-DC is significantly larger than that corresponding to CeGa-IC, thus outlining the influence of the preparation method on the surface properties of the mixed oxides. It should be stressed, however, that a straightforward correlation between the quantitative data reported in Table 2 and those suggested by the isotherms depicted in Fig. 5B is not possible because the IR absorption coefficients for the different bands occurring in the 1800–1100 cm^{-1} region are unknown.

To summarize, the results presented and discussed above clearly show that the incorporation of Ga^{3+} ions into the ceria lattice induces significant changes on the surface properties of pure ceria. Concurrently, the procedure followed in the preparation of the mixed oxide has a noticeable effect on the surface properties of

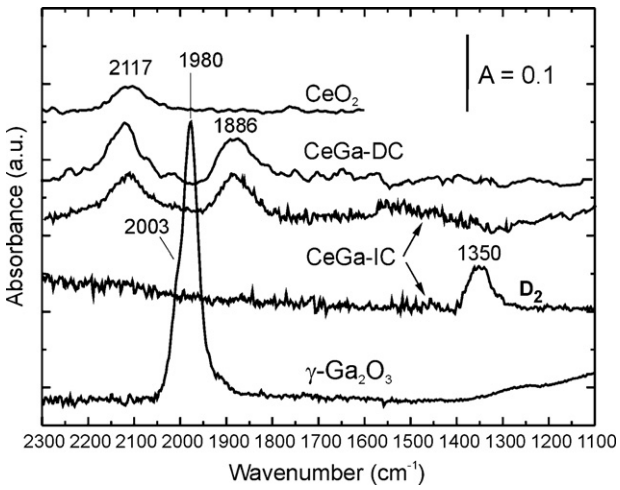

Fig. 6. Infrared spectra for $H_2(D_2)$ chemisorption at 723 K on γ-Ga_2O_3, CeO_2, CeGa-DC and CeGa-IC samples.

CeGa-IC and CeGa-DC samples. In general, all the results of the adsorption of CO_2 and CO over the of pure and mixed oxides investigated in this work point to that the incorporation of gallium into the ceria structure may lower the surface basicity of the ceria, producing more labile carbonates surface groups.

4.2. Adsorption of H_2

The adsorption of molecular hydrogen on the different materials was studied by in situ FTIR. Fig. 6 depicts the IR spectra obtained under flowing pure H_2 (D_2) at 723 K.

The spectrum recorded for CeO_2 shows a very characteristic band at 2117 cm^{-1}, which in accordance with the literature [30], may be assigned to a forbidden electronic transition of the cation Ce^{3+} ($^2F_{5/2} \rightarrow {}^2F_{7/2}$). The intensity of this signal may thus be correlated with the reduction degree reached by ceria. In the case of gallia, the spectrum reported in Fig. 6 shows two overlapped bands at 2003 and 1980 cm^{-1} which can be assigned to the stretching Ga-H mode in reduced gallium cations with tetrahedral [$\nu(Ga^{IV}$-H)] and octahedral [$\nu(Ga^{VI}$-H)] coordination, respectively [13].

Regarding the mixed oxide samples, the spectra recorded at 723 K, under flowing H_2, clearly show the signal corresponding to Ce^{3+} at 2117 cm^{-1}, and a second band at approximately 1886 cm^{-1}. As in the case of the Ga-H bands in pure Ga_2O_3, the latter feature was easily removed by 5 min evacuation at 723 K, which could suggest a similar chemical nature. However, the band recorded on the mixed oxides is red shifted by some 100 cm^{-1} with respect to that observed on Ga_2O_3. To confirm the assignation of the band at 1886 cm^{-1} to a Ga-H stretching mode, we have run a parallel adsorption experiment on the CeGa-IC sample in which D_2 was used instead of H_2. As deduced from the corresponding spectrum, Fig. 6(D_2), no band at 1886 cm^{-1} is observed. Instead, a new feature at 1350 cm^{-1} may be noticed. If the ratio between the wavenumbers corresponding to the band at 1886 cm^{-1}, tentatively assigned to a stretching mode of Ga-H, and that for the new one at 1350 cm^{-1}, 1.40, is compared with the theoretical ratio corresponding to the isotopic substitution Ga-H(D), ν(Ga-H)/ν(Ga-D) = $(\mu GaD/\mu GaH)^{1/2}$ = 1.40, where μGaD and μGaH stand for the reduced mass of the GaD and GaH species, an excellent agreement is found. This observation supports the assignment of the band at 1886 cm^{-1} to the stretching mode of the Ga-H bond in the cerium-gallium mixed oxide. The strong red shift of this band with respect to the position at which it is observed in pure gallia may thus be interpreted as a clear indication of the different chemical environment for the gallium sites in the mixed oxide. This, in turn, lends further support to the incorporation of gallium into the fluorite structure of ceria.

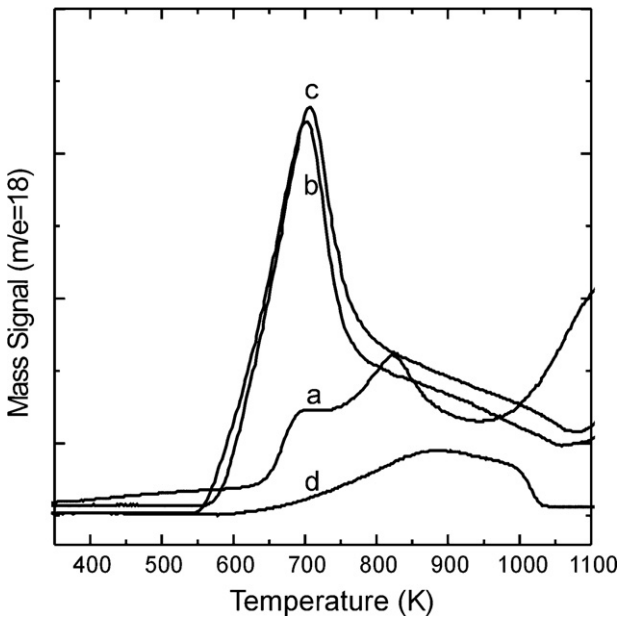

Fig. 7. TPR-H_2 study on CeO_2 (a), CeGa-DC (b), CeGa-IC (c) and γ-Ga_2O_3 (d) samples.

4.3. H_2- and CO-temperature programmed reduction

The redox behavior of the ceria–gallia mixed oxides has been characterized by means of TPR-MS. Experiments under flowing 5% H_2/Ar and 5% CO/He were run. The use of both reducing agents actually provides us with complementary information [25]. In accordance with the comparative study of reducibility against H_2 and CO of two ceria–zirconia samples carried out in [25], two major differences may be noticed between the oxide responses against each of the assayed reductants. The first one would reflect the intrinsic thermodynamic difference of reducing power existing between H_2 and CO. There is, however, a second, very relevant, difference. It is related to the mechanism of the reduction process. As shown in [31], in the case of H_2, the rate-determining step of the overall reduction process actually consists of the dissociative adsorption of H_2. As a result, the corresponding TPR trace, at least to the lowest temperature range (T = 773 K) of it, is kinetically determined by the activation of H_2 at the surface of the mixed oxide [31]. In the case of CO, the reduction mechanism is obviously different, the kinetic control, though still existing [25], being significantly more relaxed than in the case of the parallel H_2 process.

The TPR-H_2 diagrams recorded for the whole set of oxide samples are depicted in Fig. 7. The trace for pure gallia is characterized by a low-intensity broad and ill resolved feature starting at 600 K, which reaches its maximum at approximately 870 K. Regarding the diagram for pure ceria, water evolution starts to be observed at 650 K with a shoulder at 700 K and a maximum at 830 K, which is followed by an additional reduction step, at higher temperature, that could not be fully recorded under the experimental conditions applied in this work. Though still open to discussion [32,33], it is generally acknowledged that features occurring at the lowest temperatures can be assigned to surface reduction, whereas that at the highest temperature is interpreted as due to the bulk reduction of ceria [34].

The TPR-H_2 traces for DC and IC mixed oxides (Fig. 7) look like very similar, thus indicating that their response against hydrogen reduction are quite close to each other. By contrast, the profiles are significantly different from those recorded for the pure oxides:

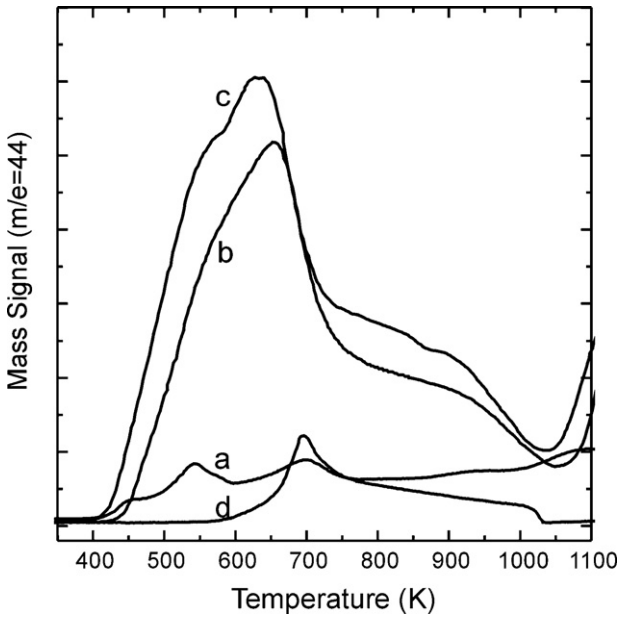

Fig. 8. TPR-CO study on CeO_2 (a), CeGa-DC (b), CeGa-IC (c) and γ-Ga_2O_3 (d) samples.

(i) the reduction starts at approximately 550 K with a maximum at 673 K and (ii) the H_2 consumption is significantly higher for DC or IC samples than for the pure oxides. We may conclude accordingly, that the incorporation of gallium into the ceria lattice strongly improves the low-temperature reducibility of the pure oxide. If we assume that, as in the case of ceria–zirconia samples [31], low-temperature reducibility is governed by the H_2 activation step, we may conclude that the dissociative chemisorption of H_2 is faster on the ceria–gallia mixed oxides.

The results of the TPR-CO study are summarized in Fig. 8. As expected [35], the diagram for Ga_2O_3 consists of a broad, low-intensity, feature peaking at 700 K. Regarding the TPR-CO diagrams for the three ceria-containing samples, we may observe that, with reference to the series of TPR-H_2 depicted in Fig. 7, the reduction under flowing 5% CO/He starts at significantly lower temperatures. Similarly, corresponding peaks are shifted towards lower temperature values with respect to those observed in the corresponding TPR-H_2 diagrams. As noted above, these effects may reasonably be interpreted as due to the kinetic difference existing between the corresponding reduction processes, much faster in the case of CO.

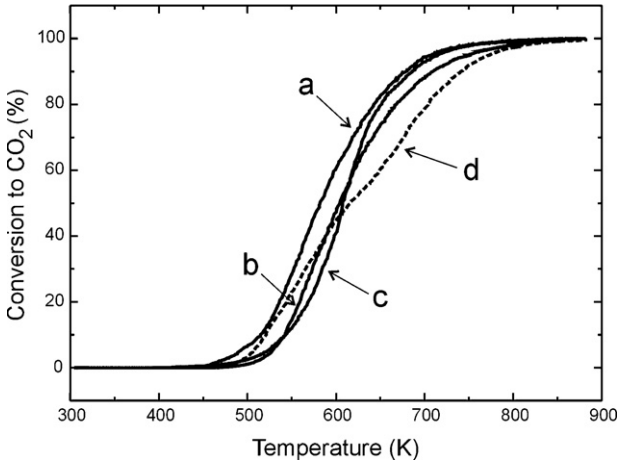

Fig. 9. Light-off curves for CO oxidation on CeO_2 (a), CeGa-DC (b), CeGa-IC (c) and $Ce_{0.32}Zr_{0.38}O_2$ (d) samples. Reaction conditions: 55 mg of solid, 1% CO + 20% O_2 (balance of He), total flow = 60 cm^3 min^{-1}, heating ramp = 10 K/min.

The comparison of Figs. 7 and 8 deserves a further comment. In effect, if we focus the attention on the diagrams b and c, i.e. those recorded for the DC and IC Ce-Ga mixed oxide samples, respectively, we may notice that traces in Figure 7 are much closer than those in Fig. 8, thus stressing the complementary nature of the TPR-H_2 and TPR-CO studies. In this particular case, the use of CO, in effect, is able to reveal the enhanced reducibility of the CeGa-IC sample with respect to that exhibited by the oxide resulting from the application of the DC preparation procedure. Accordingly, it has been highlighted in a previous section that both gallium-doped cerium oxides develop different distributions of the carbonate surface species upon exposure to CO at room temperature (see Fig. 5), which might be correlated to the said reducibility improvement of the CeGa-IC mixed oxide. Though some further studies would be necessary to fully confirm this conclusion, the different redox responses observed between IC and DC ceria–gallia samples most likely reflect subtle surface chemistry differences affecting their kinetic behavior against CO.

4.4. Catalytic test

In order to test the catalytic performance over the cerium based oxide samples, the conversion of CO was measured for the CO oxidation reaction in excess of O_2 during a heating ramp between 300 and 873 K. Fig. 9 shows the light-off curves for such experiments. Additionally, the result for CO oxidation on a commercial $Ce_{0.62}Zr_{0.38}O_2$ mixed oxide (Grace Davison, 62 m^2 g^{-1}) is included for comparison purposes. It is clear that the light-off temperatures (T_{50}, for 50% of CO conversion) are slightly different for each sample: 583, 606, and 620 K for CeO_2, CeGa-IC (or CeGa-DC) and $Ce_{0.62}Zr_{0.38}O_2$, respectively. Regardless the conversion curves for both gallium-doped ceria materials are very similar, which indicates that under our reaction conditions there is not a strong effect of the preparation method for this reaction, we can highlight that the Ce–Ga mixed oxides are, at least, as active as a conventional Ce–Zr mixed oxide for the CO oxidation reaction.

However, the higher T_{50} values of CeGa mixed oxides, as compare to our pure CeO_2, are difficult to interpret straightforward. The enhanced reducibility of the gallium-doped ceria as revealed by the TPR-CO results, that is, the oxidation of CO by lattice oxygen, seems to point in the opposite direction. Now, assuming that a redox mechanism involving lattice oxygen atoms takes place under our experimental conditions for the CO oxidation reaction, the reoxidation of the oxide is a requisite [36]. If this lattice oxygen replenishment were the rate determining step of the whole reaction, and this step were hindered over the cerium-gallium mixed oxides, it would be reasonable to expect a higher activity or lower T_{50} for ceria alone. Furthermore, it has been shown that the structure of CeO_2 has a notorious influence on the specific activity towards CO oxidation; thus, differences higher than 100 K were found between the T_{50} values for this reaction over polycrystalline CeO_2 powders by changing the ceria crystallite size [37]. Then, different factors can contribute to the observed oxidation activity on these oxides and the addition of a metal function to the oxides might also reverse this catalytic behavior.

5. Conclusions

Cerium, gallium and cerium–gallium oxides were prepared by co-precipitation with ammonium hydroxide in aqueous phase. Two Ce–Ga mixed oxides samples, with a molar nominal Ce/Ga ratio of 75/25, were obtained following direct and inverse co-precipitation procedures.

All the obtained solids, after calcination at 773 K (5 h), were mesoporous with surface areas closed to 100 m^2 g^{-1}. For both

mixed oxides, only a fluorite-type crystal structure of CeO_2 was detected; the crystallinity diminished with the presence of the Ga^{3+} cations. Different techniques suggested a quantitative incorporation of the alio-valent cation into the ceria lattice: (i) the shift of the (1 1 1) diffraction peak near 28°, (ii) the presence of oxygen vacancies revealed by Raman spectroscopy results, and (iii) the ν(Ga-H) infrared signal downshifted ca. 100 cm^{-1}.

Acid-based and redox properties of the cerium-gallium mixed oxide were characterized by CO_2 and CO chemisorption, and TPR-H_2 and TPR-CO. The formation of carbonates surface species was recorded after the chemisorption of carbon dioxide, as well carbon monoxide. It is clear that the amount of these surface species decreased after the Ga(III) doping to CeO_2. Thermal desorption also showed that the stability of these (bi)carbonates is lower in the ceria–gallia system as compared with the pure cerium dioxide. The TPR-H_2 and TPR-CO results unveiled that the redox behavior was noticeably enhanced in the gallium-doped ceria materials as compared with the pure ceria.

The catalytic activity towards the CO oxidation reaction over cerium-gallium mixed oxides was similar to the one revealed by a conventional $Ce_{0.62}Zr_{0.38}O_2$ catalyst.

Therefore, it is conclude that ceria–gallia mixed oxides are less basic and are more reducible than pure ceria. All these results point to the potential uses of metal supported catalysts on the Ce–Ga oxide system (e.g., Au or Pt/Ce–Ga–O) for the LTWGS and PROX reactions for hydrogen purification.

Acknowledgements

This work was supported by the National Council for Scientific and Technical Research (CONICET), the National Agency for the Promotion of Science and Technology (ANPCyT, Grant PICT 2005 14-33101), and Universidad Nacional del Litoral (CAID J379) of Argentina and the Agencia Española de Cooperación Internacional para el Desarrollo (AECID-MAEC) (Grant A/9621/07). Likewise, we acknowledge the financial support from MCINN of Spain/FEDER-EU (Project No. MAT2008/00889-NAN). G.F. thanks Universidad Nacional del Litoral for the research fellowship received to do her work.

References

[1] A. Trovarelli (Ed.), Catalysis by Ceria and Related Materials, Imperial College Press, London, 2002.
[2] G.C. Bond, C. Louis, D.T. Thompson (Eds.), Catalysis by Gold; Catalytic Science Series, vol. 6, World Scientific Publishing Co., London, 2006.
[3] Q. Fu, W. Deng, H. Saltsburg, M. Flytzani-Stephanopoulos, Appl. Catal. B 56 (2005) 57–68.
[4] R. Burch, Phys. Chem. Chem. Phys. 8 (2006) 5483–5500.
[5] W. Deng, M. Flytzani-Stephanopoulos, Angew. Chem. Int. Ed. 118 (2006) 2343–2347.
[6] A. Goguet, R. Burch, Y. Chen, C. Hardacre, P. Hu, R.W. Joyner, F.C. Meunier, B.S. Mun, D. Thompsett, D. Tibiletti, J. Phys. Chem. C 111 (2007) 16927–16933.
[7] A. Karpenko, Y. Denkwitz, V. Plzak, J. Cai, R. Leppelt, B. Schumacher, R.J. Behm, Catal. Lett. 116 (2007) 105–115.
[8] A. Abd El-Moemen, A. Karpenko, Y. Denkwitz, R.J. Behm, J. Power Sources 190 (2009) 64–75.
[9] S. Bernal, G. Blanco, J.M. Gatica, J.A. Pérez-Omil, J.M. Pintado, H. Vidal, G.A. Adachi, N. Imanaka, Z. Kang (Eds.), Binary Rare Earth Oxides, Kluwer Academic/Plenum Press, 2004, pp. 9–55 (Chapter 2).
[10] T. Yuzhakova, V. Rakic, C. Guimon, A. Auroux, Chem. Mater. 19 (2007) 2970–2981.
[11] B. Bonnetot, V. Rakic, T. Yuzhakova, C. Guimon, A. Auroux, Chem. Mater. 29 (2008) 1585–1596.
[12] S.E. Collins, M.A. Baltanás, A.L. Bonivardi, J. Phys. Chem. B 110 (2006) 5498–5507.
[13] S.E. Collins, M.A. Baltanás, A.L. Bonivardi, Langmuir 21 (2005) 962–970.
[14] S.E. Collins, M.A. Baltanás, A.L. Bonivardi, J. Catal. 211 (2002) 252–264.
[15] S.E. Collins, M.A. Baltanás, A.L. Bonivardi, J. Catal. 226 (2004) 410–421.
[16] M. Daturi, C. Binet, J.C. Lavalley, H. Vidal, J. Kaspar, M. Graziani, G. Blanchard, J. Chim. Phys. 95 (1998) 2048–2060.
[17] C. Otero Areán, A. López Bellan, M. Peñarroya Mentruit, M. Rodríguez Delgado, G. Turnes Palomino, Microporous Mesoporous Mater. 40 (2000) 35–42.
[18] D.-J. Kim, J. Ceram. Soc. 72 (1989) 1415–1421.
[19] D. Dohy, G. Lucazeau, A. Revcolevschi, J. Solid State Chem. 45 (1982) 180–192.
[20] J. Hanuza, M. Andruszkiewicz, Spectrochim. Acta 51A (1995) 869–881.
[21] D. Machon, P.F. McMillan, B. Xu, J. Dong, Phys. Rev. B 73 (2006) 0941251–0941259.
[22] A. Pérez Pujol, R.X. Valenzuela, A. Fuerte, E. Wloch, A. Kubacka, Z. Olejniczak, B. Sulikowski, V. Cortés Corberán, Catal. Today 78 (2003) 247–256.
[23] V.G. Keramidas, W.B. White, J. Chem. Phys. 59 (1973) 1561–1562.
[24] J.R. McBride, K.C. Hass, B.D. Poindexter, W.H. Weber, J. Appl. Phys. 76 (1994) 2435–2441.
[25] M.P. Yeste, J.C. Hernández, S. Bernal, G. Blanco, J.J. Calvino, J.A. Pérez-Omil, J.M. Pintado, Catal. Today 141 (2009) 409–414.
[26] C.D. Duprez, in: A. Trovarelli (Ed.), Catalysis by Ceria and Related Materials, Imperial College Press, London, 2002, pp. 243–280 (Chapter 7).
[27] A. Auroux, A. Gervasini, J. Phys. Chem. 94 (1990) 6371–6379.
[28] A.L. Petre, A. Auroux, P. Gélin, M. Caldararu, M.I. Ionescu, Thermochim. Acta 379 (2001) 177–185.
[29] C. Li, Y. Sakata, T. Arai, K. Domen, K. Maruya, T. Onishi, J. Chem. Soc., Faraday Trans 85 (1989) 929–943.
[30] C. Binet, A. Badri, L.-C. Lavalley, J. Phys. Chem. 98 (1994) 6392–6398.
[31] M.P. Yeste, J.C. Hernández, S. Bernal, G. Blanco, J.J. Calvino, J.A. Pérez-Omil, J.M. Pintado, Chem. Mater. 18 (2006) 2750–2757.
[32] S. Bernal, J.J. Calvino, J.M. Gatica, C. López-Cartes, J.M. Pintado, in: A. Trovarelli (Ed.), Catalysis by Ceria and Related Materials, Imperial College Press, London, 2002, pp. 85–168 (Chapter 4).
[33] F. Giordano, A. Trovarelli, C. de Leitenburg, M. Giona, J. Catal. 193 (2000) 273–282.
[34] J. El Fallah, S. Boujana, H. Dexpert, A. Kiennemann, J. Majerus, O. Touret, F. Villain, F. Le Normand, J. Phys. Chem. 98 (1994) 5522–5533.
[35] M. Haneda, E. Joubert, J.C. Ménézo, D. Duprez, J. Barbier, N. Bion, M. Daturi, J. Saussey, J.C. Lavalley, H. Hamada, Phys. Chem. Chem. Phys. 3 (2001) 1371–1375.
[36] E. Aneggi, M. Boaro, C. de Leitenburg, G. Dolcetti, A. Trovarelli, J. Alloys Compd. 408–412 (2006) 1096–1102.
[37] E. Aneggi, J. Llorca, M. Boaro, A. Trovarelli, J. Catal 234 (2005) 88–95.